

Pressure and concentration effects on intermineral calcium isotope fractionation involving garnet

Yonghui Li^{1,2}, Zhongqing Wu^{2,3,4*}, Shichun Huang⁵, Wenzhong Wang^{2,6,7}

¹ National Supercomputing Center in Chengdu, Chengdu, Sichuan 610213, China

² Laboratory of Seismology and Physics of Earth's Interior, School of Earth and Space, University of Science and Technology of China, Hefei, Anhui 230026, China

³ CAS Center for Excellence in Comparative Planetology, University of Science and Technology of China, Hefei, Anhui 230026, China

⁴ National Geophysical Observatory at Mengcheng, University of Science and Technology of China, Hefei, Anhui 230026, China

⁵ Department of Geoscience, University of Nevada, Las Vegas, NV 89154, United States

⁶ Department of Earth Sciences, University College London, London WC1E 6BT, United Kingdom

⁷ Earth and Planets Laboratory, Carnegie Institution for Science, Washington, DC 20015, USA

* Corresponding author wuzq10@ustc.edu.cn

- 1 **Key words:** Equilibrium Ca isotope fractionation, First-principles calculation, Pyrope,
- 2 Grossular, Concentration effects, Garnet, Solid solution series, Pressure effect

Abstract

To better understand the behaviors of calcium (Ca) isotopes during igneous and metamorphic processes that differentiate the Earth and other rocky planets, we investigated the pressure and effects of the Ca/Fe concentration on the average Ca–O bond length and the reduced partition function ratio of $^{44}\text{Ca}/^{40}\text{Ca}$ ($10^3\ln^{44/40}\text{Ca}\beta$) in garnet using first-principles calculations. Our calculations show that (1) the average Ca–O bond length increases with increasing Ca concentrations, significantly decreasing $10^3\ln^{44/40}\text{Ca}\beta$ (approximately 0.41‰ at 1000 K from a Ca/(Fe+Ca+Mg) of 1/24 to 12/12). In contrast to orthopyroxene and forsterite, whose Ca–O bond lengths and $10^3\ln^{44/40}\text{Ca}\beta$ are sensitive to Ca concentrations only in a narrow range, the garnet Ca–O bond length and $10^3\ln^{44/40}\text{Ca}\beta$ vary with Ca concentrations in a large range. (2) The average Ca–O bond length increases and $10^3\ln^{44/40}\text{Ca}\beta$ decreases with increasing Fe concentrations (by 0.12‰ at 1000 K, FeO content of 12.4 wt%). (3) The average Ca–O bond length decreases by ~ 0.014 Å, and $10^3\ln^{44/40}\text{Ca}\beta$ increases by 0.1‰–0.2‰ at 1000 K when the pressure increases from 0 to 3 GPa. (4) However, the pressure effect on $10^3\ln^{44/40}\text{Ca}\alpha_{\text{garnet-clinopyroxene}}$ is insignificant.

Using our new results of the pressure and effects of the Ca/Fe concentration on $10^3\ln^{44/40}\text{Ca}\alpha_{\text{garnet-clinopyroxene}}$, we evaluated the observed difference in Ca isotopes between garnet and clinopyroxene in natural samples. Most have reached equilibrium, whereas some samples exceed our prediction, which might reflect the majorite effect or kinetic fractionation.

1. Introduction

Large stable Ca isotopic variations, described using $\delta^{44/40}\text{Ca}$ ($[\frac{^{44}\text{Ca}/^{40}\text{Ca}_{\text{sample}}}{^{44}\text{Ca}/^{40}\text{Ca}_{\text{standard}}} - 1] \times 1000$), have been found in igneous and metamorphic rocks (Zhang et al., 2018; Antonelli and Simon, 2020). Some variations may reflect kinetic isotopic effects (Richter et al., 2009; Huang et al., 2010a; Watkins et al., 2011; 2014; Antonelli et al., 2019), some may reflect surface material recycling into the deep mantle (Huang et al., 2011; Amsellem et al., 2020 but see Sun et al., 2021 for a different opinion), and some may reflect equilibrium isotopic fractionation among different minerals during igneous and metamorphic processes (Huang et al., 2010b; Zhang et al., 2018; Wang et al., 2019; Zhu et al., 2021). Hence, $\delta^{44/40}\text{Ca}$ is an important tracer for understanding many geological and geochemical processes.

The behavior of Ca isotopes during igneous processes, partial melting, and crystallization under low pressure (<2 GPa) is well understood because Ca isotopic fractionation factors, among several common Ca-bearing minerals and basaltic melt, are well constrained using first-principles calculations (Wang et al., 2017a, b; Antonelli et al., 2019; Huang et al., 2019; Song et al., 2019) and measurements of natural rocks (Huang et al., 2011; Zhang et al., 2018; Wang et al., 2019). Specifically, Zhang et al. (2018) found no measurable $\delta^{44/40}\text{Ca}$ effect in melts during basaltic magma evolution and partial melting of the mantle at 0–2 GPa when garnet is not involved. However, first-principles calculations (Antonelli et al., 2019; Huang et al., 2019) and measurements of natural rocks (Antonelli et al., 2019; Kang et al., 2019; Wang et al., 2019; Chen et al., 2020; Dai et al., 2020) showed that garnets have higher $\delta^{44/40}\text{Ca}$ than coexisting clinopyroxene at equilibration. As the Ca isotopic fractionation factor between clinopyroxene-melt is close to zero (Zhang et al., 2018), one can expect a large Ca isotopic fractionation between garnet and melt, and partial melting with garnet as a

residual phase could induce large $\delta^{44/40}\text{Ca}$ variations (Wang et al., 2019). However, the effects of pressure and Ca/Fe concentrations on the reduced partition function ratio ($10^3\ln^{44/40}\text{Ca}\beta$) of garnet have not been well understood. In detail, using the first-principles approach, Antonelli et al. (2019) reported the $10^3\ln^{44/40}\text{Ca}\beta$ of garnets with three different Ca concentrations ($\text{Ca}/(\text{Ca}+\text{Mg}) = 1/23, 1/12, \text{ and } 12/12$) under zero pressure, and Huang et al. (2019) calculated the $10^3\ln^{44/40}\text{Ca}\beta$ of grossular under zero pressure. Furthermore, the Fe effect on $10^3\ln^{44/40}\text{Ca}\beta$ of garnet is poorly explored, with only one reported $10^3\ln^{44/40}\text{Ca}\beta$ for Fe-bearing garnet (almandine with $\text{Ca}/(\text{Ca}+\text{Fe}) = 1/12$; Antonelli et al., 2019).

In summary, all published first-principles studies on $10^3\ln^{44/40}\text{Ca}\beta$ of garnet were conducted at 0 GPa (Feng et al., 2014; Wang et al., 2017a, b; Antonelli et al., 2019; Song et al., 2019), leaving the pressure effect on $10^3\ln^{44/40}\text{Ca}\beta$ of garnet unexplored. Chen et al. (2020) used a simple ionic model to explore the pressure effect on $\Delta^{44/40}\text{Ca}_{\text{garnet-clinopyroxene}}$ and found that high pressure would decrease and even reverse the sign of the $\Delta^{44/40}\text{Ca}_{\text{garnet-clinopyroxene}}$. This result must be evaluated using first-principles calculations or experiments.

In this study, we used the first-principles method to systematically study the pressure and Ca/Fe concentration effects on $10^3\ln^{44/40}\text{Ca}\beta$ of garnet and analyzed our results to understand the measured $\delta^{44/40}\text{Ca}$ difference between garnets and their coexisting clinopyroxenes in natural samples.

2. Methods

2.1 First-principles calculation and $10^3\ln\beta$

Following Urey (1947) and Richet et al. (1977), the $10^3\ln^{44/40}\text{Ca}\beta$ of element X in phase A (β_A) measures the equilibrium isotope fractionation factor ($10^3\ln\alpha$) between phase A and a reference atomic gas phase. It is expressed as

$$\beta_A = \prod_i^{3N-3} \frac{u_i^*}{u_i} \frac{e^{-\frac{1}{2}u_i^*}}{(1-e^{-u_i^*})} \frac{(1-e^{-u_i})}{e^{-\frac{1}{2}u_i}}, \quad (1)$$

where i is the index of phonon modes that is $3N - 3$ for a crystal system with N atoms.

The asterisk indicates the heavy isotope, and u_i is expressed as

$$u_i = \frac{h\nu_i}{kT}, \quad (2)$$

where h and k are the Planck and Boltzmann constants, respectively, T is the temperature in Kelvin, and ν_i is the i^{th} phonon mode. The $10^3 \ln \alpha$ of element X between phases A and B can be obtained from the following equation:

$$\Delta_{A-B} = 10^3 \ln \alpha_{A-B} = 10^3 (\ln \beta_A - \ln \beta_B). \quad (3)$$

All calculations in this study were conducted using the density functional theory (DFT)-based Quantum Espresso software package, planewave basis set, and pseudopotentials (Giannozzi et al., 2009). The Mg, Al, Si, O, and Ca pseudopotentials were the same as those in our previous work (Hu et al., 2016; Wang et al., 2017a, b, Li et al., 2019a), and the Fe pseudopotential was the same as Wang et al. (2017b); thus, we could directly compare our results with our previous studies (Huang et al., 2013; Feng et al., 2014; Huang et al., 2014; Wu et al., 2015; Qin et al., 2016; Wang et al., 2017a, b; Li et al., 2019a, b). Local density approximation (LDA) was adopted to describe exchange-correlation energy (Perdew and Zunger, 1981) because of its remarkable performance in predicting the crystal volumes and vibrational properties of minerals. The energy cutoff for planewaves was 70 Rydberg (Ry). Variable cell-shape molecular dynamics (Wentzcovitch, 1991) were adopted to optimize crystal structures with k -point mesh grids, depending on the cell sizes (Fig. 1). The $1 \times 1 \times 1$ k -point was used for the Fe-free garnet with Ca/(Fe+Ca+Mg) of 1/24 and 2/24, whereas the $2 \times 2 \times 2$ k -point was used for other structures. The force, stress, and self-consistency energy

convergence were set at 10^{-4} Ry/Bohr, 0.5 Kbar, and 10^{-8} Ry, respectively. The density-functional perturbation theory was adopted to compute the phonon density of state on the gamma point for Fe-free garnets with a self-consistency threshold of 10^{-14} . DFT+U methods were applied in the structural optimization and phonon calculation of Fe-bearing garnet (PHONOPY; [Togo and Tanaka, 2015](#)). For the garnet with $\text{Fe}/(\text{Fe}+\text{Ca}+\text{Mg}) = 1/12$, a self-consistent Hubbard U value of 2.7 eV ([Cococcioni and Gironcoli, 2005](#)) was used for the only Fe atom in the cell. For the garnet with $\text{Fe}/(\text{Fe}+\text{Ca}+\text{Mg}) = 3/12$, we calculated the U values of these three Fe atoms independently because the U value depends on the local circumstances in the crystal. We obtained three similar values of 2.8, 3.0, and 3.5 eV.

2.2 Initial crystal structures

Garnet has a chemical formula of $\text{X}_3\text{Y}_2(\text{SiO}_4)_3$, where divalent cations, such as Ca^{2+} , Mg^{2+} , and Fe^{2+} , typically occupy the X site and trivalent cations, such as Al^{3+} and Fe^{3+} , occupy the Y site. End-members pyrope ($\text{Mg}_3\text{Al}_2(\text{SiO}_4)_3$) and grossular ($\text{Ca}_3\text{Al}_2(\text{SiO}_4)_3$) have a space group of Ia-3d, and they form a complete solid solution series ([Du et al., 2015](#)). The initial crystal structures of pyrope ([Gibbs and Smith, 1965](#)) and grossular ([Novak and Gibbs, 1971](#)) were downloaded from the American Mineralogist Crystal Structure Database. Conventional pyrope and grossular cells have 8 chemical formulas with 160 atoms that can be transformed into 80-atom primitive cells. The structures of Fe-free garnet with $\text{Ca}/(\text{Fe}+\text{Ca}+\text{Mg})$ of 1/24 and 2/24 were constructed from the 160-atom cell, and other configurations were generated from the 80-atom cell to reduce the computing cost. [Wang et al. \(2017a\)](#) showed that the cell size has a limited effect on the calculated average Ca–O bond length and $10^3 \ln^{44/40}\text{Ca}\beta$.

For Fe-free Ca-doped pyropes, we replaced Mg atoms in the crystals with Ca atoms to achieve different $\text{Ca}/(\text{Fe}+\text{Ca}+\text{Mg})$ ratios. For example, we replaced one Mg

atom with one Ca atom in a 160-atom pyrope to construct the initial crystal structure of Ca-doped pyrope with a $\text{Ca}/(\text{Fe}+\text{Ca}+\text{Mg})$ of 1/24. Similarly, we constructed the initial structures of Fe-free garnets with $\text{Ca}/(\text{Fe}+\text{Ca}+\text{Mg})$ of 2/24, 2/12, 3/12, 4/12, 6/12, 8/12, 9/12, and 11/12, which were well relaxed within LDA in our calculations. Each Fe-free garnet had several nonequivalent configurations, and the configuration with the lowest total energy was chosen for phonon calculations. To evaluate the Fe effect on the structures and $10^3 \ln^{44/40\text{Ca}} \beta$ of Ca, we used Fe atoms to replace one or three Mg atoms in the most stable structure with $\text{Ca}/(\text{Fe}+\text{Ca}+\text{Mg})$ of 2/12 to construct the initial structures of Fe-bearing garnets with $\text{Fe}/(\text{Fe}+\text{Ca}+\text{Mg})$ of 1/12 and 3/12. All configurations were optimized using the LDA+U method, and the configuration with the lowest total energy was selected for phonon calculations. We evaluated the pressure effect by calculating the structures and $10^3 \ln^{44/40\text{Ca}} \beta$ of garnets at 3 GPa with six different Ca/Fe concentrations, i.e., $\text{Ca}/(\text{Fe}+\text{Ca}+\text{Mg}) = 1/24, 2/12, 6/12, 12/12$, and $\text{Fe}/(\text{Fe}+\text{Ca}+\text{Mg}) = 1/12, 3/12$, grossular at 5 and 10 GPa, and garnet with $\text{Ca}/(\text{Fe}+\text{Ca}+\text{Mg}) = 1/24$ at 10 GPa. We also investigated the structures and $10^3 \ln^{44/40\text{Ca}} \beta$ of diopside at 3 and 10 GPa, and clinopyroxene with $\text{Ca}/(\text{Ca}+\text{Mg}) = 5/8$ at 3 GPa to complement the initial study of clinopyroxene at 0 GPa by [Wang et al. \(2017a\)](#), allowing a direct comparison of our first-principles results to measurements of garnet–clinopyroxene pairs in natural samples.

3. Results

3.1 Relaxed crystal structures, predicted frequencies, and the Ca–O bond length

The calculated pyrope and grossular vibrational frequencies correlate well with the Raman and infrared (IR) spectroscopy measurements of natural samples ([Fig. 2](#)). At 0 GPa, the calculated pyrope and grossular volumes at static conditions are ~2%

smaller than the experimental data under ambient conditions (Gibbs and Smith, 1965; Novak and Gibbs, 1971). The zero-point motion and room temperature effects that were ignored in static calculations increase the pyrope and grossular volumes by ~2% (Hu et al., 2016; Duan et al., 2019). Considering these two factors, our predicted volumes agree with the experimental volumes within 0.5% (Fig. 3a). The Ca concentration dependence of volume at 0 GPa is also well described using the LDA calculations, showing an increasing tendency with increasing Ca concentrations, similar to the experimental data. These agreements (Fig. 2, 3a; Table 1) show that the LDA calculations can well predict the structure and phonon frequencies of garnets. The slope of the fitting line between our calculated and experimental frequencies is 1.000 ± 0.014 (1σ , $R^2 = 0.9998$). Based on the analysis in the study by Méheut et al. (2009), at high temperatures (>1000 K), an uncertainty of $n\%$ on phonon frequencies would induce an uncertainty of $2n\%$ on $10^3 \ln \beta$. Therefore, the relative uncertainties of our predicted $10^3 \ln \beta$ and $10^3 \ln \alpha$ are 2.8% and 4.0%, respectively.

For Fe-free garnets, the Ca–O bond lengths increase by 2.3% when the Ca/(Fe+Ca+Mg) ratio in garnet increases from 1/24 to 12/12 (Table 1 and Fig. 3b). As shown in previous studies (Feng et al., 2014; Wang et al., 2017a, b), the concentration dependence of the bond length results from the significant different radii of Mg and Ca cations. When a Mg cation in pyrope is replaced by a Ca cation, the larger Ca needs to adapt to the mineral structure mainly controlled by Mg; therefore, it forms a smaller eight-fold CaO_8 polyhedron in pyrope than in grossular. The Ca–O bond length is a function of Ca concentration when Ca/(Fe+Ca+Mg) varies from 1/24 to 12/12 in garnets. A similar behavior was found for the Ca–O bond in carbonate minerals (Wang et al., 2017a) and the K–O bond in alkali feldspars (Li et al., 2019a). However, the Ca–O bond lengths in orthopyroxene and forsterite significantly depend on the Ca

concentration only in a narrow range ($1/48 < \text{Ca}/(\text{Fe}+\text{Ca}+\text{Mg}) < 1/8$ for orthopyroxene, and $1/64 < \text{Ca}/(\text{Fe}+\text{Ca}+\text{Mg}) < 1/8$ for forsterite).

[Table 1](#) shows the Fe effect on the average Ca–O bond length in garnets. When the $\text{Fe}/(\text{Fe}+\text{Ca}+\text{Mg})$ increases from 0 to $3/12$, the average Ca–O bond length increases from 2.351 to 2.354 Å, similar to the Fe effect on the Ca–O bond length in orthopyroxene ([Wang et al., 2017b](#)). Moreover, the average Ca–O bond lengths decrease by 0.010–0.018 Å when the pressure increases from 0 to 3 GPa for all mineral configurations ([Fig. 3c](#)), showing a slightly different pressure effect on the average Ca–O bond length of garnets with different compositions.

3.2 $10^3 \ln^{44/40}\text{Ca}\beta$ of garnet

[Fig. 4a](#) shows the temperature dependence of $10^3 \ln^{44/40}\text{Ca}\beta$ at 0 GPa, and [Table 2](#) lists their polynomial fitting parameters. All calculated $10^3 \ln^{44/40}\text{Ca}\beta$ and $10^3 \ln^{44/40}\text{Ca}\alpha$ for varying temperatures, pressures, and compositions are reported in supplementary materials. At 0 GPa, for Fe-free garnets, the Ca–O bond length increases with the increasing Ca concentration, and $10^3 \ln^{44/40}\text{Ca}\beta$ decreases significantly with the increasing Ca concentration in a wide range. This concentration dependence is also observed at 3 GPa. When $\text{Ca}/(\text{Fe}+\text{Ca}+\text{Mg})$ increases from $1/24$ to $12/12$, the $10^3 \ln^{44/40}\text{Ca}\beta$ at 1000 K decreases by 0.41‰ at 0 GPa and 0.38‰ at 3 GPa ([Fig. 4a, 4b](#); [Tables 2, 3](#)). [Antonelli et al. \(2019\)](#) found a similar relation between $10^3 \ln^{44/40}\text{Ca}\beta$ and the Ca–O bond length ([Fig. 5](#)); however, they predicted Ca–O bonds longer than those in this study because they used the generalized gradient approximation method instead of LDA. For example, for grossular at 0 GPa and static conditions, [Antonelli et al. \(2019\)](#) predicted a Ca–O bond length of 2.429 Å, compared to 2.393 Å from our study and 2.405 Å from experimental measurements ([Novak and Gibbs, 1971](#)).

[Fig. 4b](#) and [Table 3](#) show the $10^3 \ln^{44/40}\text{Ca}\alpha$ referenced to diopside. At 0 GPa, the

largest $10^3 \ln^{44/40\text{Ca}} \alpha_{\text{garnet-diopside}}$ (0.96‰ at 1000 K) is found in garnet with $\text{Ca}/(\text{Fe}+\text{Ca}+\text{Mg}) = 1/24$. For comparison, the largest $10^3 \ln^{44/40\text{Ca}} \alpha_{\text{forsterite-diopside}}$ (0.92‰ at 1000 K) and $10^3 \ln^{44/40\text{Ca}} \alpha_{\text{orthopyroxene-diopside}}$ (0.64‰ at 1000 K) are found for forsterite with $\text{Ca}/(\text{Fe}+\text{Ca}+\text{Mg}) = 1/64$ and orthopyroxene with $\text{Ca}/(\text{Fe}+\text{Ca}+\text{Mg}) = 1/48$, respectively (Wang et al., 2017b; Song et al., 2019).

$10^3 \ln^{44/40\text{Ca}} \beta$ of garnets and diopside increase from 0 GPa to 3 and 10 GPa (Table 2), respectively, showing a significant pressure effect. Specifically, $10^3 \ln^{44/40\text{Ca}} \alpha_{\text{garnet-diopside}}$ at 1000 K ranges from 0.55‰ to 0.95‰ at 10 GPa and 0.58‰ to 0.96‰ at 3 GPa (Table 3), compared to 0.55‰ to 0.96‰ at 0 GPa (Table 2).

4. Discussion

4.1 Two types of concentration effects

Our previous studies have found concentration effects on $10^3 \ln \beta$ in different isotope systems in variety of minerals, including Ca isotopes in orthopyroxene (Feng et al., 2014; Wang et al., 2017b) and forsterite (Song et al., 2019), Mg and Ca isotopes in carbonates (Wang et al., 2017a), and K isotopes in alkali feldspars (Li et al., 2019a), suggesting that the concentration effect is a ubiquitous phenomenon. There are two types of concentration effects.

Type I is represented by the $10^3 \ln^{44/40\text{Ca}} \beta$ in orthopyroxene and forsterite (Feng et al., 2014; Wang et al., 2017b; Song et al., 2019). In this type, Ca is a minor element in orthopyroxene and forsterite. Their average Ca–O bond lengths and $10^3 \ln^{44/40\text{Ca}} \beta$ vary with Ca concentrations in narrow ranges: $1/48 < \text{Ca}/(\text{Fe}+\text{Ca}+\text{Mg}) < 1/8$ for orthopyroxene, and $1/64 < \text{Ca}/(\text{Fe}+\text{Ca}+\text{Mg}) < 1/8$ for forsterite (Fig. 6). Outside this range, the average Ca–O bond length and $10^3 \ln^{44/40\text{Ca}} \beta$ are insensitive to Ca concentrations.

Type II is represented by the $10^3 \ln \beta$ of Mg isotopes in carbonates (Wang et al.,

2017a), Ca isotopes in garnet (Fig. 6), and K isotopes in alkali feldspars (Li et al., 2019a). All Type II minerals form solid solutions within a wide concentration range. Accordingly, the average Mg/Ca/K–O bond lengths and $10^3\ln\beta$ vary with Mg/Ca/K concentrations in a wide range. The range within which $10^3\ln\beta$ is sensitive to concentration is considerably narrow for Type I but extremely wide for Type II (Fig. 6).

These two types of concentration effects have two aspects in common. First, the $10^3\ln\beta$ is linearly correlated with the average bond length (Magna et al., 2015; Wang et al., 2017a, 2017b; Antonelli et al., 2019; Li et al., 2019a; Song et al., 2019). This is because $10^3\ln\beta$ is controlled by the bond strength, which is mainly determined by the bond length when the coordination number is similar. Second, both types have a low concentration limit, below which $10^3\ln\beta$ is insensitive to concentration because the local bonding environment of the atom of interest will not change significantly under extremely low concentrations; that is, below a certain concentration, the atom of interest behaves as a trace element and its bonding environment will be unaffected by the atom of interest in the neighboring cells. These lower limits are Ca/(Fe+Ca+Mg) of 1/48 for orthopyroxene (Wang et al., 2017b) and 1/64 for forsterite (Song et al., 2019). The shortest Ca–Ca distances in both cases are similar (14.11 Å for orthopyroxene and 13.89 Å for forsterite) because Ca might not interact with each other beyond this distance (14 Å). The shortest Ca–Ca distance in garnet with the lowest Ca concentration (Ca/(Mg+Ca) = 1/24) calculated in this study is 11.37 Å, which is much smaller than 14 Å. Therefore, the garnet compositions explored in this study do not reach the lower limit. The estimated lower limit for the Ca concentration below which the $10^3\ln^{44/40}\text{Ca}\beta$ of garnet is insensitive to concentration is 1/45, based on the shortest Ca–Ca distance of 14 Å.

4.2 Pressure effects on Ca–O bond length and $10^3\ln^{44/40}\text{Ca}\beta$ in garnets

Garnets under high pressures have short average Ca–O bond lengths and large $10^3 \ln^{44/40\text{Ca}}\beta$ (Table 1, 2; Fig. 3c, 3d, 5). With an increase in the pressure from 0 to 3 GPa, the average Ca–O bond length decreases from 0.010 to 0.018 Å, with an average of ~0.014 Å for all configurations, corresponding to a slope of approximately -0.0047 Å/GPa (Table 1; Fig. 3c). This pressure dependence extends to high pressures that increase from 0 to 3, 5, and 10 GPa, when the average Ca–O bond length of grossular linearly decreases from 2.393 to 2.377, 2.368, and 2.345 Å, respectively, with a slope of approximately -0.0047 Å/GPa, which is similar to previous reports of 0.004 and 0.0049 Å/GPa (Hazen and Finger, 1978; Akhmatkaya et al., 1999). We can summarize Ca–O bond lengths ($L(\text{Ca-O})$) as a function of pressure and Ca/Fe concentration as follows:

$$\begin{aligned}
 L(\text{Ca-O}) &= B_2 X^2 + B_1 X + B_0 + g(F) \\
 g(F) &= (0.144 - 0.012 \times P) \times F^2 - (0.024 - 0.0038 \times P) \times F \\
 B_2 &= -0.0482 - 0.0036 \times P \\
 B_1 &= 0.1019 + 0.0046 \times P \\
 B_0 &= 2.3366 - 0.0054 \times P
 \end{aligned} \tag{4}$$

All calculated garnet configurations have larger $10^3 \ln^{44/40\text{Ca}}\beta$ at 3 GPa than those at 0 GPa with slightly different increasing rates (Fig. 3d). We also summarize $10^3 \ln^{44/40\text{Ca}}\beta$ (at 1000 K, ‰) of garnets using different Ca/Fe concentrations below 3 GPa as

$$\begin{aligned}
 10^3 \ln^{44/40\text{Ca}}\beta &= C_2 X^2 + C_1 X + C_0 - f(F) \\
 f(F) &= -(0.837 + 1.0601 \times P) \times F^2 + (0.6974 + 0.3563 \times P) \times F \\
 C_2 &= 0.6992 - 0.0824 \times P \\
 C_1 &= -1.1147 + 0.0768 \times P \\
 C_0 &= 2.4158 + 0.0462 \times P
 \end{aligned} \tag{5}$$

where $X = \text{Ca}/(\text{Fe}+\text{Ca}+\text{Mg})$ from 0 to 1, $f(F)$ and $g(F)$ are the effects of Fe on $10^3 \ln^{44/40\text{Ca}}\beta$ and the average Ca–O bond length, respectively, $F = \text{Fe}/(\text{Fe}+\text{Ca}+\text{Mg})$ from 0 to 0.25 (with FeO contents below 12.4 wt%), and P is the pressure ranging from 0 to

3 GPa. It is assumed that the effect of Fe on $10^3 \ln^{44/40}\text{Ca}\beta$ and the average Ca–O bond length is only the function of Fe concentration and pressure, regardless of Ca/(Fe+Ca+Mg) (Wang et al., 2017b).

The calculated six garnets with different Ca/Fe concentrations have slightly varying slopes of $10^3 \ln^{44/40}\text{Ca}\beta$ with pressures from 0.034‰/GPa to 0.064‰/GPa at 1000 K (Table 2; Fig. 3d). Furthermore, when the pressure increases to 5 and 10 GPa, $10^3 \ln^{44/40}\text{Ca}\beta$ of grossular increases linearly, giving an average slope of ~0.040‰/GPa at 1000 K (Table 2; Fig. 3d). Therefore, $10^3 \ln^{44/40}\text{Ca}\beta$ of grossular without Fe concentrations at 1000 K can be summarized as follows:

$$10^3 \ln \beta = 1.997 + 0.040 \times P \quad (6)$$

Below 10 GPa, the Ca concentration effects on $10^3 \ln^{44/40}\text{Ca}\beta$ of garnets do not vary with pressure (Table 2, 3). At 0 GPa, the variations in $10^3 \ln^{44/40}\text{Ca}\beta$ caused by Ca concentrations are 0.41‰ at 1000 K, 0.38‰ at 3 GPa, and 0.40‰ at 10 GPa.

Our calculation shows a limited pressure effect on the intermineral Ca isotope fractionation factor ($10^3 \ln^{44/40}\text{Ca}\alpha_{\text{garnet-clinopyroxene}}$) (Fig. 7a, 7b) because of the similar pressure effects on $10^3 \ln^{44/40}\text{Ca}\beta$ of garnet and clinopyroxene. Our calculation shows that the slope of $10^3 \ln^{44/40}\text{Ca}\beta$ at 1000 K in diopside is ~0.040‰/GPa, comparable with garnets (from 0.034‰/GPa to 0.064‰/GPa). Particularly, this diopside slope is similar to those of grossular and garnet with Ca/(Fe+Ca+Mg) = 1/24 (0.040‰/GPa and 0.039‰/GPa, respectively). Therefore, $10^3 \ln^{44/40}\text{Ca}\alpha_{\text{garnet-diopside}}$ at 1000 K is near-constant, regardless of pressure (0.55‰ at 0 and 10 GPa for grossular, 0.96‰ at 0 GPa and 0.95‰ at 10 GPa for garnet with Ca/(Fe+Ca+Mg) = 1/24). In summary, the $10^3 \ln^{44/40}\text{Ca}\alpha_{\text{garnet-clinopyroxene}}$ varies with Ca concentrations in garnet and clinopyroxene, but not pressure.

4.3 Implications for Ca isotope fractionation in natural samples

Wang et al. (2019) reported Ca isotope compositions in garnet–clinopyroxene pairs separated from eclogites and garnet peridotites of the Dabie orogeny, China. They argued that the studied garnet–clinopyroxene pairs could have reached isotope equilibrium based on coarse-grained granular textures (Liu et al., 2015), homogeneous mineral compositions (Li et al., 2011), and homogeneous Ca isotopic compositions of the individual minerals on a grain scale (Wang et al., 2019). Consequently, they attributed the observed composition- $\Delta^{44/40}\text{Ca}_{\text{garnet-clinopyroxene}}$ correlation (Fig. 7) to a mineral composition effect. In detail, Wang et al. (2019) found that $A_{\text{garnet-clinopyroxene}}$ of $^{44}\text{Ca}/^{40}\text{Ca}$ (intermineral isotope fractionation corrected for temperature effect, $A_{\text{garnet-clinopyroxene}} = \Delta^{44/40}\text{Ca}_{\text{garnet-clinopyroxene}} \times T^2/10^6$, T is the temperature in Kelvin) negatively correlates with $\text{Ca}/(\text{Fe}+\text{Ca}+\text{Mg})$ in garnet (Fig. 7b) and the jadeite content in clinopyroxene (Wang et al., 2019). Assuming that $10^3\ln^{44/40}\text{Ca}\beta$ of garnet is independent of its Ca concentration when $\text{Ca}/(\text{Fe}+\text{Ca}+\text{Mg})$ is $>1/8$, Wang et al. (2019) speculated that the clinopyroxene jadeite content mostly caused the $A_{\text{garnet-clinopyroxene}}$ variation. However, $10^3\ln^{44/40}\text{Ca}\beta$ of garnet varies with Ca concentrations in a wide range (Type II, see Section 4.1), different from the concentration dependence of $10^3\ln^{44/40}\text{Ca}\beta$ of orthopyroxene (Type I). As shown in Fig. 7a and 7b, the pressure and Ca concentration effects on $10^3\ln^{44/40}\text{Ca}\beta$ of garnet can explain most of the compositional dependence of $A_{\text{garnet-clinopyroxene}}$ reported by Wang et al. (2019).

In a Na-free system, the Ca–O bond length and $10^3\ln^{44/40}\text{Ca}\beta$ in clinopyroxene also depend on its Ca concentration (Wang et al., 2017b). Clinopyroxene with $\text{Ca}/(\text{Ca}+\text{Mg}) = 4/8$ has the longest Ca–O bond length and, hence, the smallest $10^3\ln^{44/40}\text{Ca}\beta$. A deviation from $\text{Ca}/(\text{Ca}+\text{Mg}) = 4/8$ will decrease the Ca–O bond length and increase $10^3\ln^{44/40}\text{Ca}\beta$. At 1000 K, $10^3\ln^{44/40}\text{Ca}\beta$ increases by 0.14‰ from clinopyroxene with

Ca/(Ca+Mg) = 4/8 to clinopyroxene with Ca/(Ca+Mg) = 5/8. Considering the pressure and Ca/Fe concentration effects in garnet and Na-free clinopyroxene, we provide a possible range of $10^3 \ln^{44/40}\text{Ca} \alpha_{\text{garnet-clinopyroxene}}$ as a function of temperature with upper and lower limits (Fig. 7a), enveloping most of the published garnet–clinopyroxene pairs (Antonelli et al., 2019; Kang et al., 2019; Wang et al., 2019; Dai et al., 2020). Especially, using the Ca, Mg, and Fe contents of garnet and clinopyroxene from ZMF-3 (Wang et al., 2019), we predict an $A_{\text{garnet-clinopyroxene}}$ of $^{44}\text{Ca}/^{40}\text{Ca}$ of 0.69‰, which matches well with the measured value of $0.66 \pm 0.07\%$. These results indicate that (1) $\Delta^{44/40}\text{Ca}_{\text{garnet-clinopyroxene}}$ is controlled by both garnet and clinopyroxene compositions as well as temperature; and (2) most garnet–clinopyroxene pairs in published studies (Antonelli et al., 2019; Kang et al., 2019; Wang et al., 2019; Dai et al., 2020) likely reached Ca isotope equilibrium.

Chen et al. (2020) reported $\delta^{44/40}\text{Ca}$ of garnet–clinopyroxene pairs from Roberts Victor eclogites. The $\Delta^{44/40}\text{Ca}_{\text{garnet-clinopyroxene}}$ observed in Roberts Victor eclogites range from negative to positive values (Fig 7a), and the temperature-corrected intermineral fractionation factors ($A_{\text{garnet-clinopyroxene}}$) negatively correlate with Ca/(Fe+Ca+Mg) in garnet (Fig. 7b). However, such a large variation in $A_{\text{garnet-clinopyroxene}}$ cannot be fully explained by equilibrium intermineral isotope fractionation based on our first-principles calculations (Fig. 7b), even after considering the effects of pressure and Ca/(Fe+Ca+Mg) variations in garnet and clinopyroxene. According to our calculations, with the increasing pressure, the $10^3 \ln^{44/40}\text{Ca} \beta$ of garnet increases with slopes of 0.034‰/GPa–0.064‰/GPa, whereas clinopyroxene increases with slopes of 0.040‰/GPa–0.043‰/GPa. The pressure effects on $10^3 \ln^{44/40}\text{Ca} \beta$ for garnets and clinopyroxene are similar in size and identical in direction; therefore, $A_{\text{garnet-clinopyroxene}}$ is insensitive to pressure. For comparison, $A_{\text{grossular-diopside}}$ is 0.55‰ at 10 and 0 GPa

(Table 3). The equilibrium pressures of the samples studied by Chen et al. (2020) range from 3 to 6.9 GPa. However, such pressure variation cannot explain the $A_{\text{garnet-clinopyroxene}}$ variations reported by them (Fig. 7b).

Significantly, two types of Roberts Victor eclogites are reported by Chen et al. (2020): Type I and Type II. For the Type I samples, their $\Delta^{44/40}\text{Ca}_{\text{garnet-clinopyroxene}}$ and $A_{\text{garnet-clinopyroxene}}$ fit our first-principles calculations well (Fig. 7a, 7b; light blue down triangles). The Type II samples show larger $\Delta^{44/40}\text{Ca}_{\text{garnet-clinopyroxene}}$ and $A_{\text{garnet-clinopyroxene}}$ variations, even from negative to positive (Fig. 7a, 7b; light gray down triangles). Three reasons exist for the large $A_{\text{garnet-clinopyroxene}}$ variation observed in Type II Roberts Victor eclogite samples reported by Chen et al. (2020).

First, the higher positive $\Delta^{44/40}\text{Ca}_{\text{garnet-clinopyroxene}}$ might inherit from the $\Delta^{44/40}\text{Ca}_{\text{majorite-clinopyroxene}}$ under higher pressure. The Ca concentrations of these higher positive $\Delta^{44/40}\text{Ca}_{\text{garnet-clinopyroxene}}$ data range from 0.1 to 0.2 (Fig. 7b). Because majorite has a much higher SiO_2 content than garnet, we might find quartz or coesite in samples if the garnet in samples was transformed from majorite. Petrographic features of Type II eclogites show localized silica on the edges of some garnet grains (Fig. 1A-5 in Gréau et al., 2011); therefore, the $\Delta^{44/40}\text{Ca}_{\text{garnet-clinopyroxene}}$ of Type II eclogites might reflect the original $\Delta^{44/40}\text{Ca}_{\text{majorite-clinopyroxene}}$. Huang et al. (2013) reported that majorite has a shorter Mg–O bond length than pyrope at 0 GPa; therefore, the Ca–O bond length of Ca-doped majorite might be shorter than in pyrope, resulting in much higher $10^3 \ln^{44/40}\text{Ca}\beta$ than garnet. However, $10^3 \ln^{44/40}\text{Ca}\beta$ of majorite was not studied and needs more focus.

Second, the negative $\Delta^{44/40}\text{Ca}_{\text{garnet-clinopyroxene}}$ might reflect a higher jadeite component in clinopyroxene under higher pressure, increasing $10^3 \ln^{44/40}\text{Ca}\beta_{\text{clinopyroxene}}$ (Wang et al., 2019). However, Chen et al. (2020) found no correlation between

$\Delta^{44/40}\text{Ca}_{\text{garnet-clinopyroxene}}$ and jadeite proportions in clinopyroxene (see their Fig. S4). Particularly, the Roberts Victor eclogite sample, RV07-34, with the most negative $\Delta^{44/40}\text{Ca}_{\text{garnet-clinopyroxene}}$ (-0.31%) has a clinopyroxene jadeite proportion of $\sim 40\%$. In comparison, Dabie granitoid samples with jadeite proportions of $\sim 40\%$ have positive $\Delta^{44/40}\text{Ca}_{\text{garnet-clinopyroxene}}$ (0.48% – 0.81%) (Wang et al., 2019). The effect of jadeite components on $\Delta^{44/40}\text{Ca}_{\text{garnet-clinopyroxene}}$ must be better constrained.

Third, the large $\Delta^{44/40}\text{Ca}_{\text{garnet-clinopyroxene}}$ variations in Type II Roberts Victor eclogites may reflect a kinetic isotope effect (Zhao et al., 2017; Antonelli et al., 2019). Therefore, these Roberts Victor eclogite garnet–clinopyroxene pairs (Chen et al., 2020) have not reached Ca isotope exchange equilibrium.

5. Conclusions

We investigated the structures and $10^3\ln^{44/40}\text{Ca}\beta$ of garnets with different Ca/Fe concentrations and pressures using first-principles calculations. Our calculated results well described the dependence of volume on Ca concentrations and the vibrational properties of garnet. At 0 GPa, the average Ca–O bond length increases from 2.340 to 2.393 Å and $10^3\ln^{44/40}\text{Ca}\beta$ at 1000 K decreases from 2.40‰ to 1.99‰, with the Ca concentration Ca/(Fe+Ca+Mg) increasing from 1/24 to 12/12. At 0 GPa, with Fe/(Fe+Ca+Mg) increasing from 0 to 3/12 (Ca/(Fe+Ca+Mg) = 2/12), the average Ca–O bond length increases from 2.351 to 2.354 Å and the $10^3\ln^{44/40}\text{Ca}\beta$ at 1000 K decreases from 2.25‰ to 2.13‰. For all configurations, the average Ca–O bond length decreases with the pressure from 0.0034 to 0.006 Å/GPa and $10^3\ln^{44/40}\text{Ca}\beta$ increases from 0.034‰/GPa to 0.064‰/GPa.

Furthermore, we found limited $10^3\ln^{44/40}\text{Ca}\alpha_{\text{garnet-clinopyroxene}}$ variations under 0 (0.55% – 0.96% at 1000 K) and 3 GPa (0.58% – 0.96% at 1000 K), reflecting near-zero pressure effects on $10^3\ln^{44/40}\text{Ca}\alpha_{\text{garnet-clinopyroxene}}$. Especially, at 10 GPa, our calculation

gives $10^3 \ln^{44/40\text{Ca}} \alpha_{\text{grossular-diopside}}$ of 0.55‰ at 1000 K, the same as the value at 0 GPa.

Combined with our previous work, two types of concentration effects were identified. In Type I, Ca in orthopyroxene and forsterite is a minor or trace element and the Ca–O bond length and $10^3 \ln^{44/40\text{Ca}} \beta$ vary in a narrow Ca concentration range ($1/48 < \text{Ca}/(\text{Fe}+\text{Ca}+\text{Mg}) < 1/8$ for orthopyroxene and $1/64 < \text{Ca}/(\text{Fe}+\text{Ca}+\text{Mg}) < 1/8$ for forsterite). However, in Type II, Ca in garnet, carbonate minerals, and K in alkali feldspars are major elements and the Ca/K–O bond lengths and $10^3 \ln^{44/40\text{Ca}} \beta$ vary in a significantly wide concentration range. Both types show a good linear relation between the average bond length and $10^3 \ln^{44/40\text{Ca}} \beta$.

Considering the effects of pressure and Ca/Fe concentrations in garnet and clinopyroxene, we estimated the upper and lower limits of $10^3 \ln^{44/40\text{Ca}} \alpha_{\text{garnet-clinopyroxene}}$. The difference between the upper and lower limits is 0.66‰ at 1000 K. Some reported $\Delta^{44/40}\text{Ca}_{\text{garnet-clinopyroxene}}$ in natural samples fall within our estimated $10^3 \ln^{44/40\text{Ca}} \alpha_{\text{garnet-clinopyroxene}}$, indicating that their $\Delta^{44/40}\text{Ca}_{\text{garnet-clinopyroxene}}$ reflects equilibrium intermineral isotope fractionation controlled by temperature, pressure, and the compositions of clinopyroxene and garnet. The abnormally high and low $\Delta^{44/40}\text{Ca}_{\text{garnet-clinopyroxene}}$ data might show the majorite, jadeite effects, and kinetic isotope fractionation.

Acknowledgment

This study is supported by the Strategic Priority Research Program (B) of the Chinese Academy of Sciences (XDB41000000), National Key R&D Program of China (2018YFA0702703), and National Natural Science Foundation of China (41721002, 41925017). SH acknowledges support from NSF EAR-1942042. The calculations were partly conducted at supercomputing center of USTC.

References

- Akhmatskaya E., Nobes R., Milman V. and Winkler B. (1999) Structural properties of garnets under pressure: an first principles study. *Zeitschrift für Kristallographie-Crystall. Mater.* **214**, 808-819.
- Amsellem E., Moynier F., Bertrand H., Bouyon A., Mata J., Tappe S., Day J.M.D. (2020) Calcium isotopic evidence for the mantle sources of carbonatites. *Sci. Adv.* **6**, eaba3269.
- Antonelli M.A., Brown S.T., Simon J.I. (2020) Calcium isotopes in high-temperature terrestrial processes. *Chem. Geol.* **548**, 119651.
- Antonelli M.A., Schiller M., Schauble E.A., Mittal T., DePaolo D.J., Chacko T., Grew E.S. and Tripoli B. (2019) Kinetic and equilibrium Ca isotope effects in high-T rocks and minerals. *Earth Planet. Sci. Lett.* **517**, 71-82.
- Asimow P.D., Ghiorso M.S (1998) Algorithmic Modifications Extending MELTS to Calculate Subsolvus Phase Relations. *Am. Mineral.* **83**, 1127-1131.
- Chen C.F., Huang J.X., Foly S.F., Wang Z.C., Moynier F., Liu Y., Dai W., Li M. (2020) Compositional and pressure controls on calcium and magnesium isotope fractionation in magmatic systems. *Geochim. Cosmochim. Acta.* **290**, 257-270.
- Cococcioni M. and Gironcoli S. (2005) Linear response approach to the calculation of the effective interaction parameters in the LDA+U method. *Phys. Rev. B.* **71** 035105.
- Dai W., Wang Z., Liu Y., Chen C., Zong K., Zhou L., Zhang G., Li M., Moynier F. and Hu Z. (2020) Calcium isotope compositions of mantle pyroxenites. *Geochim. Cosmochim. Acta* **270**, 144-159.
- Du W., Clark S. M. & Walker D. (2015) Thermo-compression of pyrope-grossular garnet solid solutions: Non-linear compositional dependence. *Am. Mineral.* **100**(1), 215-222.
- Du W., Han B., Clark S.M., Wang Y. and Liu Y. (2017) Raman spectroscopic study of synthetic pyrope-grossular garnet: structural implications. *Phys Chem Minerals.* **45**, 197-209.
- Duan L., Wang W., Wu Z., Qian W. (2019) Thermodynamic and Elastic Properties of Grossular at High Pressures and High Temperatures: A First-Principles Study. *J. Geophys. Res.* **124**, 7792-7805.
- Feng C, Qin T, Huang S, Wu Z, Huang F. (2014) First-principles investigations of equilibrium calcium isotope fractionation between clinopyroxene and Ca-doped orthopyroxene. *Geochim. Cosmochim. Acta.* **143**, 132-142.
- Giannozzi P., Baroni S., Bonini N., Calandra M., Car R., Cavazzoni C., Ceresoli D., Chiarotti G. L., Cococcioni M., Dabo I., Dal Corso A., de Gironcoli S., Fabris S., Fratesi G., Gebauer R., Gerstmann U., Gougoussis C., Kokalj A., Lazzeri M., Martin-Samos L., Marzari N., Mauri F., Mazzarello R., Paolini S., Pasquarello A., Paulatto L., Sbraccia C., Scandolo S., Sclauzero G., Seitsonen A. P., Smogunov A., Umari P. and Wentzcovitch R. M. (2009) QUANTUM ESPRESSO: a modular and open-source software project for quantum simulations of materials. *J. Phys. Condens. Matter* **21**, 395502.
- Gibbs G. V. and Smith J. V. (1965) Refinement of the crystal structure of synthetic pyrope, refinement D, note that temperature factors reported for Si were labelled, incorrectly in the paper. *Am. Mineral.* **50**, 2023-2039.
- Gréau Y., Huang J. X., Griffin W. L., Renac C., Alard O. and O'Reilly S. Y. (2011) Type I eclogites from Roberts Victor kimberlites: products of extensive mantle metasomatism. *Geochim. Cosmochim. Acta* **75**, 6927-6954.
- Hazen R. M. and Finger L. W. (1978) Crystal structures and compressibilities of pyrope

- and grossular to 60 kbar. *Am. Mineral.* **63**, 297-303.
- Hofmeister A. M., Fagan T. J., Campbell K. M., & Schaal R. B. (1996) Single-crystal IR spectroscopy of pyrope-almandine garnet with minor amounts of Mn and Ca. *Am. Mineral.* **81**, 418-428.
- Hu Y., Wu Z., Dera P. K. and Bina C. R. (2016) Thermodynamic and elastic properties of pyrope at high pressure and high temperature by first-principles calculations, *J. Geophys. Res. Sol. Ea.* **121**, 6462-6476.
- Huang F., Chakraborty P., Lundstrom C.C., Holmden C., Glessner J.J.G., Kieffer S.W. & Lesher C.E. (2010a) Isotope fractionation in silicate melts by thermal diffusion. *Nature.* **464**, 396-400.
- Huang F., Chen L., Wu Z. and Wang W. (2013) First-principles calculations of equilibrium Mg isotope fractionations between garnet, clinopyroxene, orthopyroxene, and olivine: implications for Mg isotope thermometry. *Earth Planet. Sci. Lett.* **367**, 61-70.
- Huang F., Chen Z., Wang W., Kang J., Wu Z. (2019) First-principles calculations of equilibrium Ca isotope fractionation: Implications for oldhamite formation and evolution of lunar magma ocean. *Earth Planet. Sci. Lett.* **510**, 153-160.
- Huang F., Wu Z., Huang S. and Wu F. (2014) First-principles calculations of equilibrium silicon isotope fractionation among mantle minerals. *Geochim. Cosmochim. Acta.* **140**, 509-520.
- Huang, S., Farkaš, J., Jacobsen, S.B. (2010b) Calcium isotopic fractionation between clinopyroxene and orthopyroxene from mantle peridotites. *Earth Planet. Sci. Lett.* **292**, 337-344.
- Huang, S., Farkaš, J., Jacobsen, S.B. (2011) Stable calcium isotopic compositions of Hawaiian shield lavas: evidence for recycling of ancient marine carbonates into the mantle. *Geochim. Cosmochim. Acta* **75**, 4987-4997.
- Hudspeth J., Sanloup C., Kono Y. (2018) Properties of molten CaCO₃ at high pressure. *Geochem. Persp. Let.* **7**, 17-21.
- Kang J. T., Ionov D. A., Zhu H. L., Liu F., Zhang Z. F., Liu Z. and Huang F. (2019) Calcium isotope sources and fractionation during melt-rock interaction in the lithospheric mantle: Evidence from pyroxenites, wehrlites, and eclogites. *Chem. Geol.* **524**, 272-282.
- Li W.-Y., Teng F.-Z., Xiao Y. and Huang J. (2011) Hightemperature inter-mineral magnesium isotope fractionation in eclogite from the Dabie orogen, China. *Earth Planet. Sci. Lett.* **304**, 224-230.
- Li Y., Wang W., Huang S., Wang K and Wu Z. (2019a) First-principles investigation of the concentration effect on equilibrium fractionation of K isotopes in feldspars. *Geochim. Cosmochim. Acta.* **245**, 374-384.
- Li Y., Wang W., Wu Z. and Huang S. (2019b) First-principles investigation of equilibrium K isotope fractionation among K-bearing minerals. *Geochim. Cosmochim. Acta.* **264**, 30-42.
- Liu S.-A., Huang J., Liu J., Wörner G., Yang W., Tang Y.-J., Chen Y., Tang L., Zheng J. and Li S. (2015) Copper isotopic composition of the silicate Earth. *Earth Planet. Sci. Lett.* **427**, 95-103.
- Magna T., Gussone N., Mezger K. (2015) The calcium isotope systematics of Mars. *Earth Planet. Sci. Lett.* **430**, 86-94.
- McAloon B. P., Hofmeister A. M. (1995) Single-crystal IR spectroscopy of grossular-andradite garnet, *Am. Mineral.* **80**, 1145-1156.
- Méheut M., Lazzeri M., Balan E. and Mauri F. (2009) Structural control over equilibrium silicon and oxygen isotopic fractionation: a first-principles density-

- functional theory study. *Chem. Geol.* **258**, 28-37.
- Novak G. A. and Gibbs G. V. (1971) The crystal chemistry of the silicate garnet sample Gr. *Am. Mineral.* **56**, 791-825.
- Perdew J. P. and Zunger A. (1981) Self-interaction correction to density-functional approximations for many-electron systems. *Phys. Rev. B* **23**, 5048–5079.
- Qin T., Wu F., Wu Z. and Huang F. (2016) First-principles calculations of equilibrium fractionation of O and Si isotopes in quartz, albite, anorthite, and zircon. *Contrib. Mineral. Petrol.* **171**, 91.
- Richet P., Bottinga Y. and Javoy M. (1977) Review of hydrogen, carbon, nitrogen, oxygen, sulfur, and chlorine stable isotope fractionation among gaseous molecules. *Annu. Rev. Earth Planet. Sci.* **5**, 65–110.
- Richter F.M., Watson E.B., Mendybaev R., Dauphas N., Georg B., Watkins J., Valley J. (2009) Isotopic fractionation of the major elements of molten basalt by chemical and thermal diffusion. *Geochim. Cosmochim. Acta* **73**, 4250-4263.
- Rustad J. R. and Yin Q.-Z. (2009) Iron isotope fractionation in the Earth's lower mantle. *Nat. Geosci.* **2**, 514-518.
- Song Y. H., Li Y. H., Wu Z. Q., Wang W. Z. (2019) First-principles investigation of the concentration effect on equilibrium fractionation of Ca isotopes in forsterite. *Acta Geochim.* **38**(4), 497-507.
- Sun J., Zhu X.-K., Belshaw N.S., Chen W., Doroshkevich A.G., Luo W.-J., Song W.-L., Chen B.-B., Cheng Z.-G., Li Z.-H., Wang Y., Kynicky J., Henderson G.M. (2021) Ca isotope systematics of carbonatites: Insights into carbonatite source and evolution. *Geochem. Persp. Lett.* **17**, 11-15.
- Togo A. and Tanaka I. (2015) First principles phonon calculations in materials science. *Scr. Mater.* **108**, 1-5.
- Urey H. C. (1947) The thermodynamic properties of isotopic substances. *J. Chem. Soc. (Lond.)*, 562-581.
- Wang W., Qin T., Zhou C., Huang S., Wu Z., Huang F. (2017a) Concentration effect on equilibrium fractionation of Mg-Ca isotopes in carbonate minerals: Insights from first-principles calculations. *Geochim. Cosmochim. Acta.* **208**, 185-197.
- Wang W., Zhou C., Qin T., Kang J., Huang S., Wu Z., Huang F. (2017b) Effect of Ca content on equilibrium Ca isotope fractionation between orthopyroxene and clinopyroxene. *Geochim. Cosmochim. Acta.* **219**, 44-56.
- Wang Y., He Y., Wu H., Zhu C., Huang S. and Huang J. (2019) Calcium isotope fractionation during crustal melting and magma differentiation: Granitoid and mineral-pair perspectives. *Geochim. Cosmochim. Acta.* **259**, 37-52.
- Watkins J.M., Liang Y., Richter F., Ryerson F.J., DePaolo D.J. (2014) Diffusion of multi-isotopic chemical species in molten silicates. *Geochim. Cosmochim. Acta* **139**, 313-326.
- Watkins J.M., DePaolo D.J., Ryerson F.J., Peterson B.T. (2011) Influence of liquid structure on diffusive isotope separation in molten silicates and aqueous solutions. *Geochim. Cosmochim. Acta* **75**, 3103-3118.
- Wentzcovitch R. M. (1991) Invariant molecular-dynamics approach to structural phase transitions. *Phys. Rev. B.* **44**, 2358-2361.
- Wu Z., Huang F. and Huang S. (2015) Isotope fractionation induced by phase transformation: first-principles investigation for Mg₂SiO₄. *Earth Planet. Sci. Lett.* **409**, 339–347.
- Zhang H., Wang Y., He Y., Teng F.-Z., Jacobsen S.B., Helz R.T., Marsh B.D., Huang S. (2018) No measurable calcium isotopic fractionation during crystallization of Kilauea Iki lava lake. *Geochem. Geophys. Geosyst.* **19**, 3128-3139.

- Zhao X., Zhang Z., Huang S., Liu Y., Li X. & Zhang H. (2017) Coupled extremely light Ca and Fe isotopes in peridotites. *Geochim. Cosmochim. Acta.* **208**, 368-380.
- Zhu H., Liu F., Li X., Wang G., Zhang Z. and Sun W. (2018) Calcium isotopic compositions of normal mid-ocean ridge basalts from the southern Juan de Fuca ridge. *J. Geophys. Res. Solid Earth* **123**, 1303–1313.
- Zhu H, Liao R, Liu H, Du L, Li H, Li C, Zhang Z, Sun W. (2021) Calcium isotopic fractionation during magma differentiation: Constraints from volcanic glasses from the eastern Manus Basin, *Geochim. Cosmochim. Acta.* **305**, 228-242.

1 **Tables**

2 **Table 1.** The average Ca–O bond lengths (Å) with different Ca/(Fe+Ca+Mg),
 3 Fe/(Fe+Ca+Mg) and pressures.

Minerals	Ca/(Fe+Ca+ Mg)	Fe/(Fe+Ca+ Mg)	Average bond lengths (Å)		
			Ca–O	Exp.	CN
0 GPa					
	1/24	0	2.340		8
	2/24	0	2.345		8
	2/12	0	2.351		8
	2/12	1/12	2.350		8
	2/12	3/12	2.354		8
	3/12	0	2.359		8
	4/12	0	2.367		8
	6/12	0	2.379		8
	8/12	0	2.381		8
	9/12	0	2.383		8
	11/12	0	2.388		8
Grossular	12/12	0	2.393	2.405 ^a	8
Clinopyroxene	4/8	0	2.470 ^b		8
	5/8	0	2.453 ^c		7.6
3 GPa					
	1/24	0	2.326		8
	2/12	0	2.336		8
	2/12	1/12	2.336		8
	2/12	3/12	2.340		8
	6/12	0	2.365		8
Grossular	12/12	0	2.377		8
Clinopyroxene	4/8	0	2.449		8
	5/8	0	2.419		7.6
5 GPa					
Grossular	12/12	0	2.368		8
10 GPa					
	1/24	0	2.298		8
Grossular	12/12	0	2.345		8
Clinopyroxene	4/8	0	2.404		8

4 Data sources:

5 ^a [Novak and Gibbs. \(1971\)](#)

6 ^b [Feng et al. \(2014\)](#)

7 ^c [Wang et al. \(2017b\)](#)

8

9 **Table 2.** The polynomial fitting parameters of $10^3 \ln^{44/40}\text{Ca}\beta$ in garnet, orthopyroxene,
 10 clinopyroxene, and forsterite with different Ca/(Fe+Ca+Mg), Fe/(Fe+Ca+Mg), and
 11 pressure versus temperature.

	Ca/(Fe+Ca +Mg)	Fe/(Fe+Ca +Mg)	A	B	C
0 GPa					
	1/24	0	2.41413	-0.01416	1.77E-04
	2/24	0	2.33948	-0.01367	1.73E-04
	2/12	0	2.26390	-0.01258	1.53E-04
	2/12	1/12	2.21102	-0.01198	1.44E-04
	2/12	3/12	2.14049	-0.01116	1.29E-04
	3/12	0	2.14381	-0.01158	1.42E-04
	4/12	0	2.12123	-0.01132	1.39E-04
	6/12	0	2.04826	-0.01068	1.30E-04
	8/12	0	2.02069	-0.01074	1.31E-04
	9/12	0	2.00452	-0.01069	1.31E-04
	11/12	0	1.98405	-0.01065	1.31E-04
Grossular	12/12	0	1.99699	-0.01069	1.33E-04
Orthopyroxene	1/48 ^a	0	2.10389	-0.01324	1.94E-04
	4/8 ^b	0	1.44228	-0.00674	9.53E-05
Clinopyroxene	5/8 ^a	0	1.57108	-0.00792	1.04E-04
Forsterite	1/64 ^c	0	2.38261	-0.01573	2.36E-04
3 GPa					
	1/24	0	2.51793	-0.01507	1.93E-04
	2/12	0	2.45814	-0.01481	1.90E-04
	2/12	1/12	2.33728	-0.0132	1.60E-04
	2/12	3/12	2.26527	-0.01234	1.43E-04
	6/12	0	2.22656	-0.01245	1.58E-04
Grossular	12/12	0	2.13614	-0.01208	1.56E-04
Clinopyroxene	4/8	0	1.55513	-0.00742	1.02E-04
	5/8	0	1.70249	-0.00910	1.21E-04
5 GPa					
Grossular	12/12	0	2.21970	-0.01360	1.76E-04
10 GPa					
	1/24	0	2.40159	-0.01542	2.02E-04
Grossular	12/12	0	2.40159	-0.01540	2.02E-04
Clinopyroxene	4/8	0	1.84132	-0.01000	1.39E-04

12 The polynomial fitting function: $10^3 \ln\beta = Ax + Bx^2 + Cx^3$, where x is $10^6/T^2$ and
 13 T is the temperature in Kelvin. The fitting temperature range is between 400 K and
 14 2475 K. All data are provided in supplementary materials.

15 Data sources:

16 ^a [Wang et al. \(2017b\)](#)

17 ^b [Feng et al. \(2014\)](#)

18 ^c [Song et al. \(2019\)](#)

Table 3. The polynomial fitting parameters of $10^3 \ln^{44/40}\text{Ca} \alpha$ between minerals (garnet, orthopyroxene, and forsterite) and diopside (Fe-free clinopyroxene with Ca/(Ca+Mg) of 4/8) with different Ca/(Fe+Ca+Mg), Fe/(Fe+Ca+Mg), and pressure versus temperature.

	Ca/(Fe+Ca +Mg)	Fe/(Fe+Ca +Mg)	A	B	C
0 GPa					
	1/24	0	0.97185	-0.00742	8.17E-05
	2/24	0	0.89720	-0.00692	7.80E-05
	2/12	0	0.82163	-0.00583	5.76E-05
	2/12	1/12	0.76874	-0.00524	4.90E-05
	2/12	3/12	0.69821	-0.00442	3.37E-05
	3/12	0	0.70153	-0.00484	4.70E-05
	4/12	0	0.67895	-0.00457	4.36E-05
	6/12	0	0.60599	-0.00394	3.45E-05
	8/12	0	0.57841	-0.00399	3.62E-05
	9/12	0	0.56224	-0.00395	3.62E-05
	11/12	0	0.54177	-0.00390	3.52E-05
Grossular	12/12	0	0.55471	-0.00395	3.74E-05
Orthopyroxene	1/48	0	0.66161	-0.00650	9.91E-05
Clinopyroxene	5/8	0	0.12880	-0.00118	8.79E-06
Forsterite	1/64	0	0.94033	-0.00899	1.41E-04
3 GPa					
	1/24	0	0.96280	-0.00765	9.11E-05
	2/12	0	0.90302	-0.00739	8.78E-05
	2/12	1/12	0.78216	-0.00578	5.74E-05
	2/12	3/12	0.71014	-0.00492	4.12E-05
	6/12	0	0.67143	-0.00503	5.55E-05
Grossular	12/12	0	0.58102	-0.00466	5.37E-05
Clinopyroxene	5/8	0	0.14737	-0.00168	1.85E-05
10 GPa					
	1/24	0	0.96228	-0.00917	1.18E-04
Grossular	12/12	0	0.56027	-0.00542	6.27E-05

The polynomial fitting function: $10^3 \ln \alpha = Ax + Bx^2 + Cx^3$, where x is $10^6/T^2$ and T is the temperature in Kelvin. The fitting temperature range is between 400 K and 2475 K. All data are provided in supplementary materials.

Figure captions

Figure 1. Crystal structures of pyrope-grossular solid solutions with different Ca/(Fe+Ca+Mg) and Fe/(Fe+Ca+Mg).

Figure 2. Calculated phonons (vibrational frequencies) of pyrope and grossular compared to experimental Raman and IR spectroscopy measurements. The Raman data of pyrope and grossular are from [Du et al. \(2017\)](#). The IR data of pyrope are from [Hofmeister et al. \(1996\)](#), and the grossular data are from [McAloon and Hofmeister \(1995\)](#).

Figure 3. At 0 GPa, the cell volumes (a) and average Ca–O bond lengths (b) of Fe-free garnets as a function of garnet Ca/(Fe+Ca+Mg) ratios. The pressure effects on the average Ca–O bond length (c) and $10^3 \ln^{44/40}\text{Ca}\beta$ (d). The diamonds, squares, upper, and lower triangles in figure (a) are experimental data. [Hu et al. \(2016\)](#) and [Duan et al. \(2019\)](#) have calculated the volumes of Fe-free pyrope and grossular at ambient conditions by including vibrational contributions to the volume using the same methods (QE software, local density approximation, and the same pseudopotentials). The volume correction for other Ca concentrations is the weighted mean value of volume correction of pyrope and grossular from [Hu et al. \(2016\)](#) and [Duan et al. \(2019\)](#).

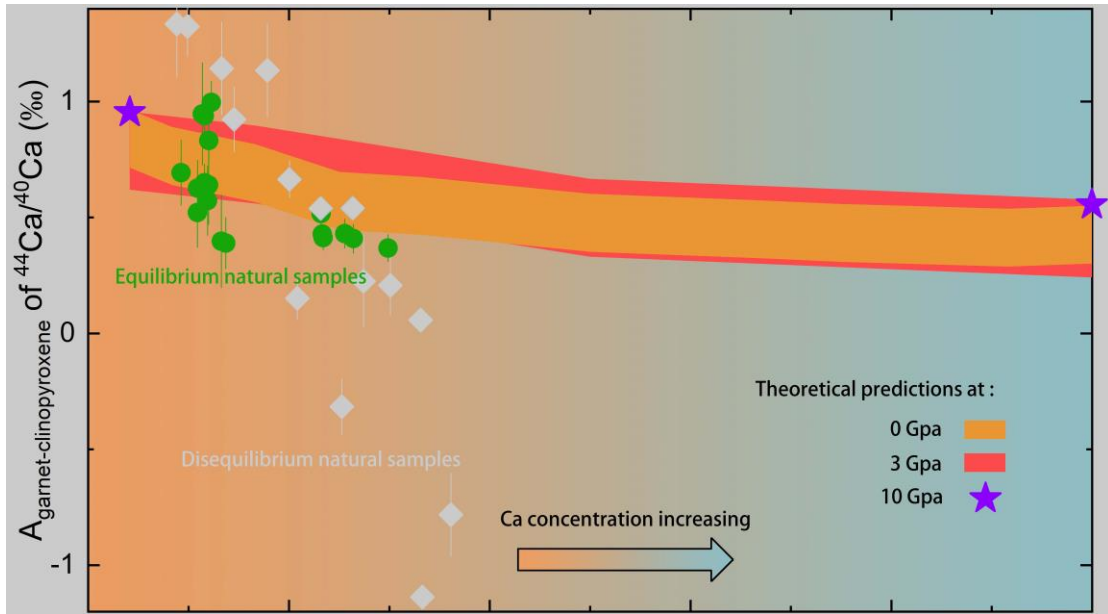
Figure 4. At 0 GPa, $10^3 \ln^{44/40}\text{Ca}\beta$ (a) and $10^3 \ln^{44/40}\text{Ca}\alpha$ between minerals (garnet, orthopyroxene, and forsterite) and diopside (Fe-free clinopyroxene with Ca/(Fe+Ca+Mg) of 4/8) (b) as a function of temperature. Ca/(Fe+Ca+Mg) for Fe-free minerals are labeled at the right edge of the graph. The data of forsterite are from [Song et al. \(2019\)](#) and orthopyroxene from [Wang et al. \(2017b\)](#). For Fe-bearing garnet, their Fe[Ca]/(Fe+Ca+Mg) are shown in the legend.

Figure 5. Correlation between $10^3 \ln^{44/40}\text{Ca}\beta$ at 1000 K and the average Ca–O bond length of Fe-free garnets with different pressures. The results reported by [Antonelli et al. \(2019\)](#) (red dots, 0 GPa) using GGA and our results using a LDA are plotted on one line within analytic error. GGA typically shows a longer bond length than LDA. The uncertainty reported by [Antonelli et al. \(2019\)](#) is 6%, referred from the scale factor they used (1.06, see their supplementary material). The labels show the Ca/(Fe+Ca+Mg) ratios.

Figure 6. $10^3 \ln^{44/40}\text{Ca}\alpha_{\text{X-diopside}}$ (a) and the average Ca–O bond length (b) as a function of Ca/(Fe+Ca+Mg) among upper mantle minerals (Fe-free forsterite,

orthopyroxene, clinopyroxene, and garnet).

Figure 7. (a) The possible region of $10^3 \ln^{44/40\text{Ca}} \alpha_{\text{garnet-clinopyroxene}}$ caused by pressure and temperature. (b) $A_{\text{garnet-clinopyroxene}}$ of $^{44}\text{Ca}/^{40}\text{Ca}$ varies with pressure and Ca/Fe concentrations in garnets. $A_{\text{garnet-clinopyroxene}} = \Delta^{44/40}\text{Ca}_{\text{garnet-clinopyroxene}} \times T^2/10^6$. The pressure effects are evaluated based on our calculations in [Table 2](#) and [3](#). The Fe concentration effects on $10^3 \ln^{44/40\text{Ca}} \alpha_{\text{garnet-clinopyroxene}}$ of garnets are assumed to be the same as that in the configuration with Ca/(Fe+Ca+Mg) of 2/12. With Fe/(Fe+Ca+Mg) increasing from 0 to 3/12, the effect on $10^3 \ln^{44/40\text{Ca}} \beta$ in garnet at 0 and 3 GPa were evaluated from [Table 2](#). The garnet-1/24 indicates the garnet with Ca/(Fe+Ca+Mg) = 1/24.



Graphical Abstract

1
2
3
4
5

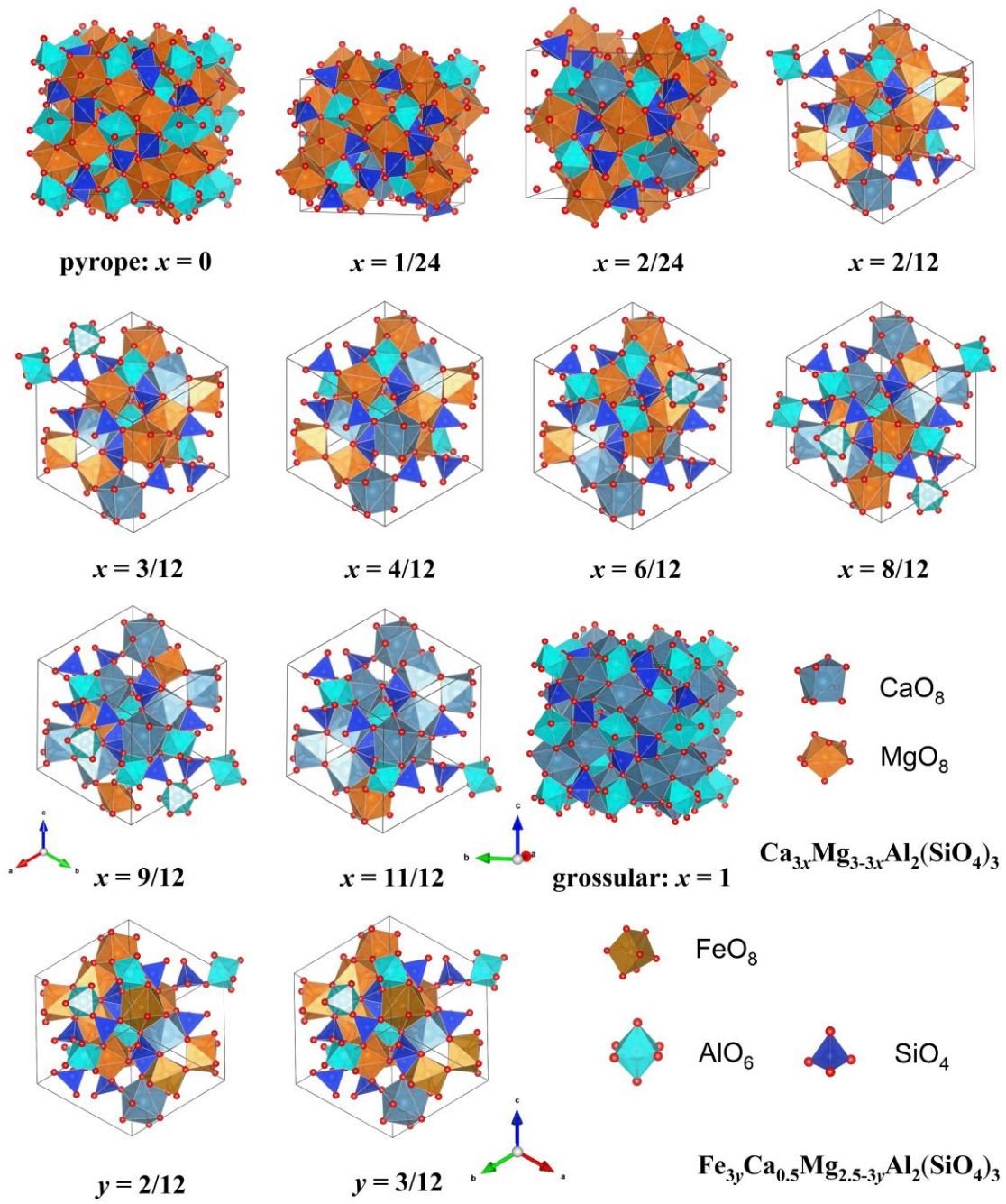


Figure 1

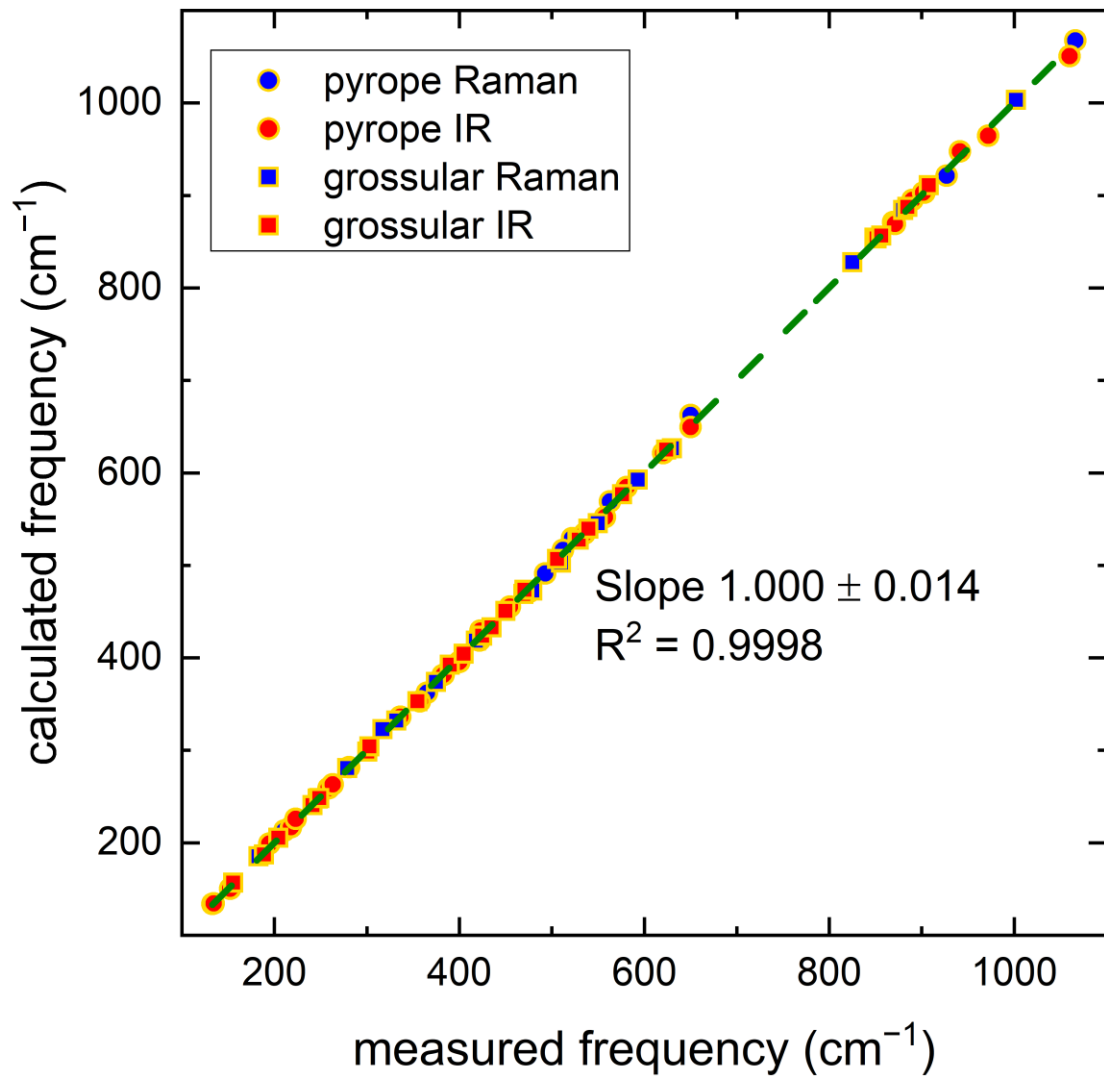


Figure 2

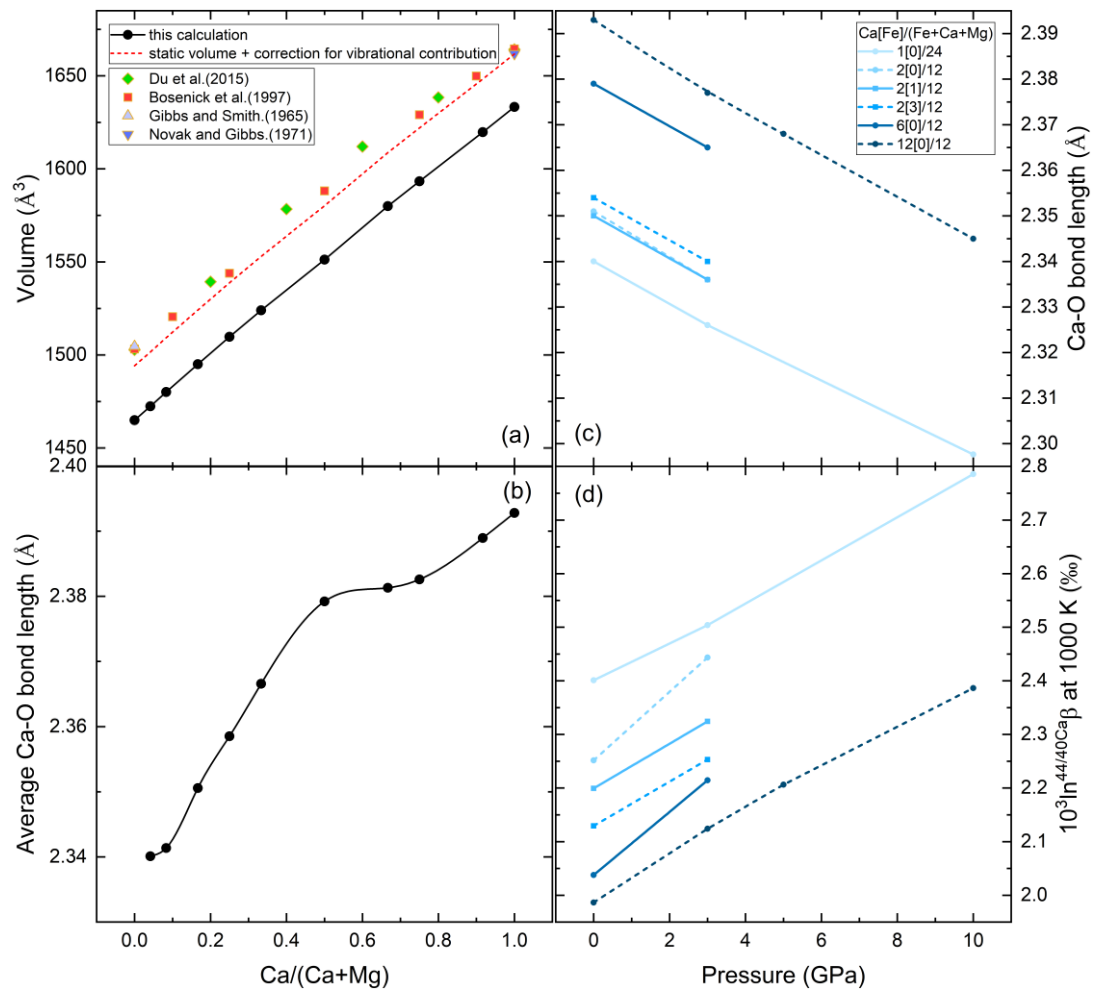


Figure 3

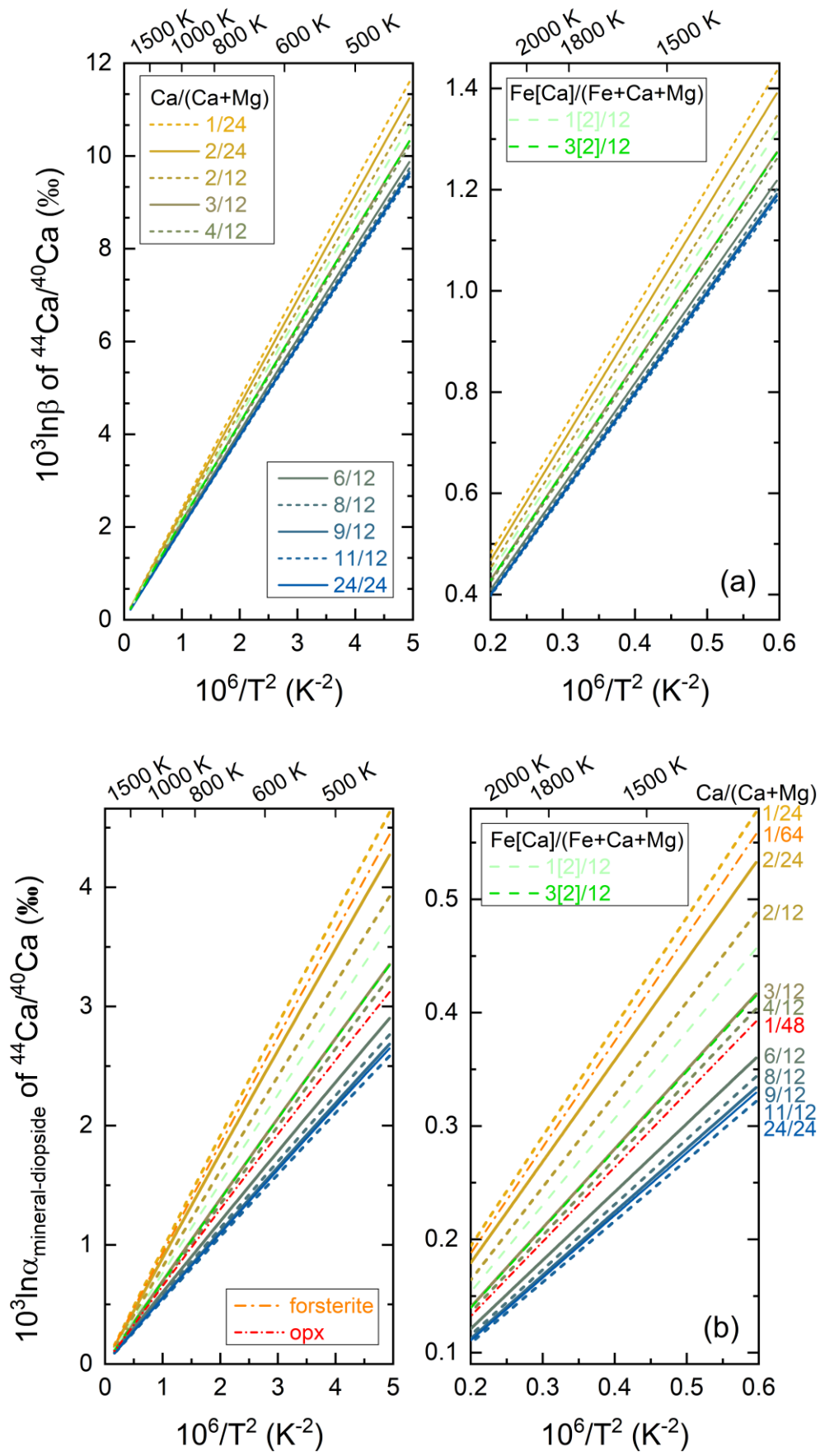


Figure 4

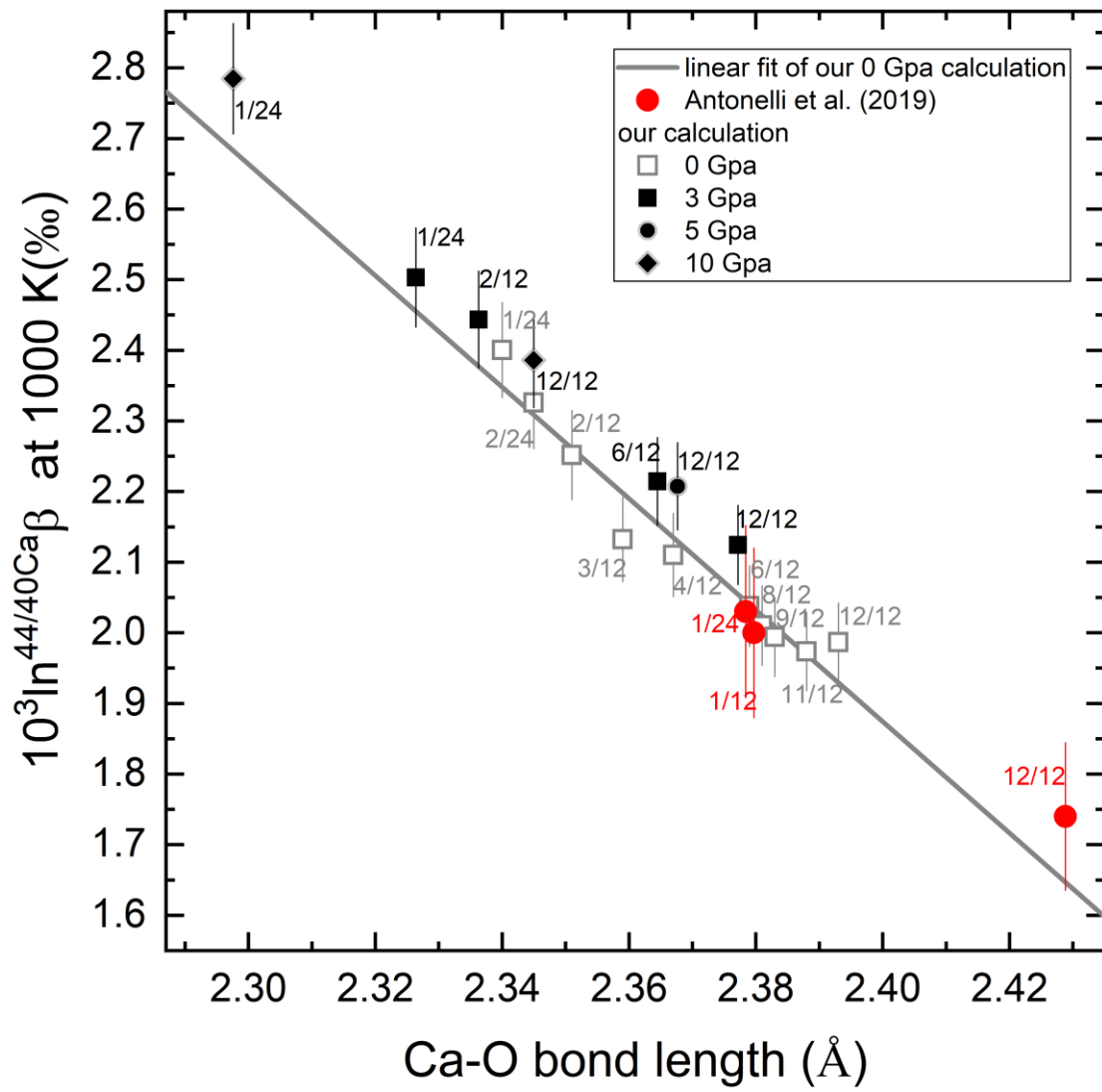


Figure 5

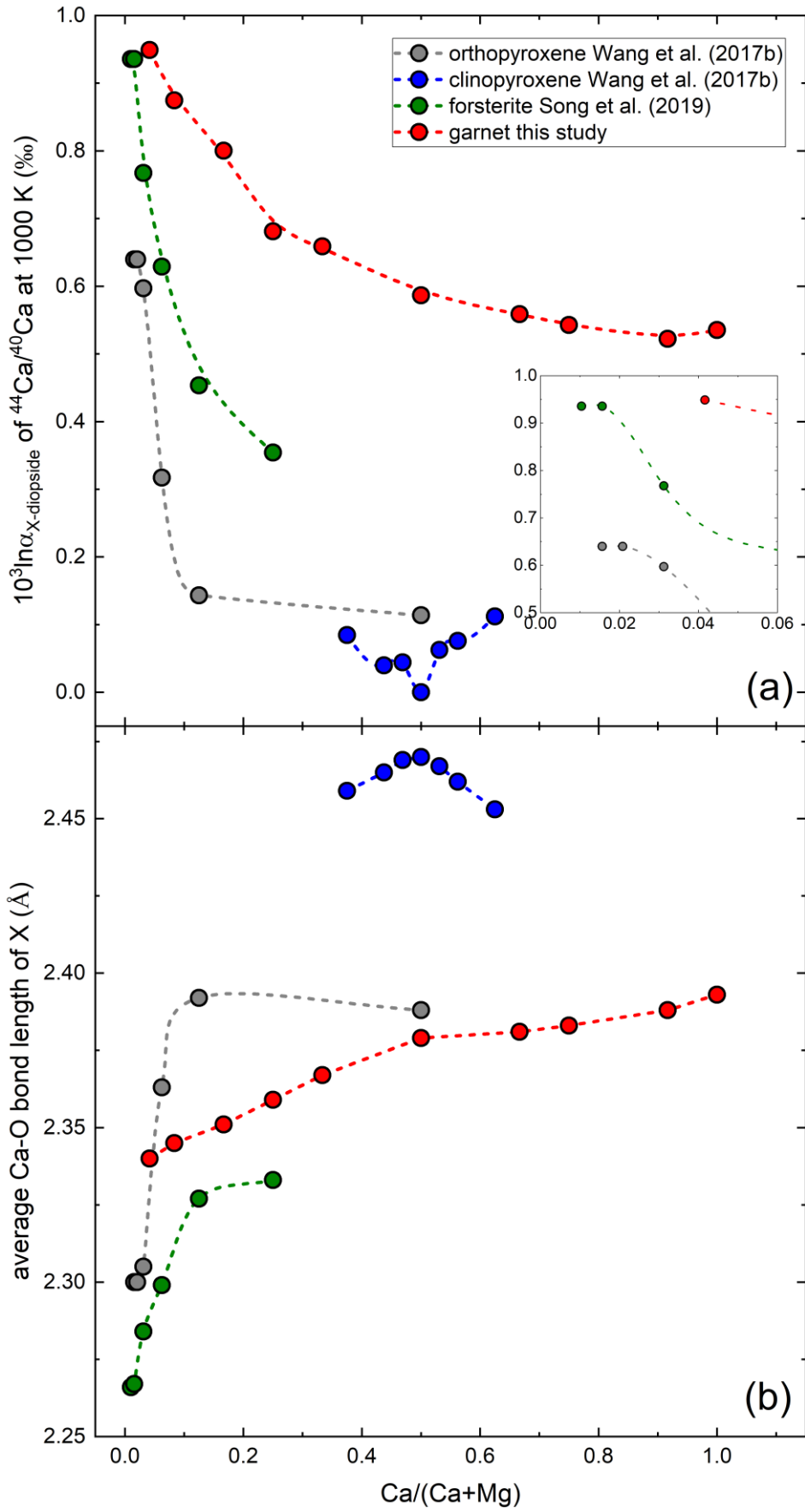
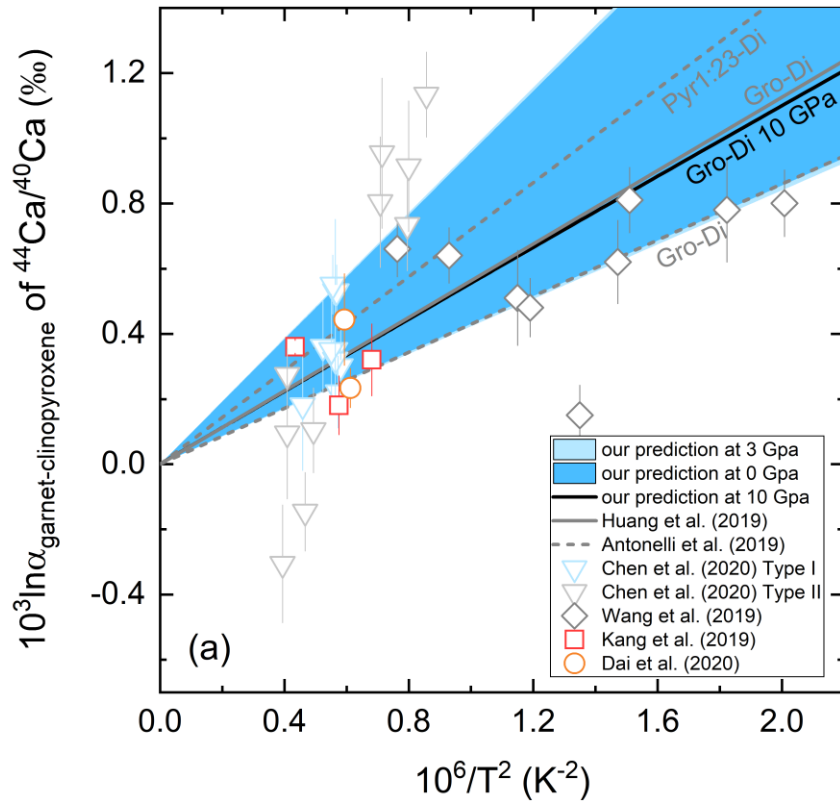
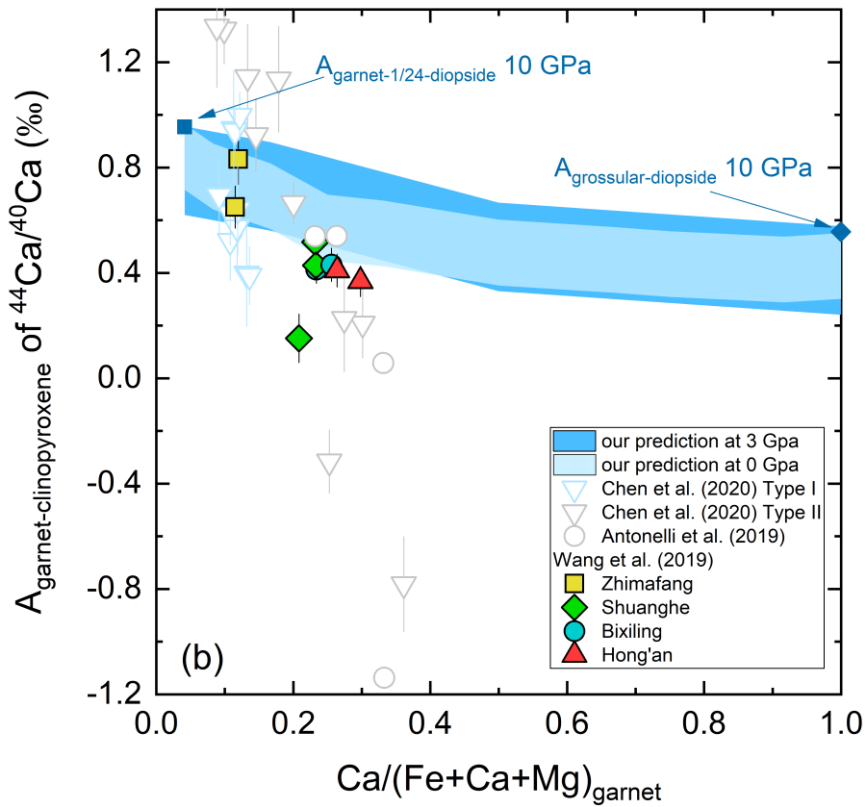


Figure 6



1



2

3

4

Figure 7